Copyright © 2008 Tech Science Press SDHM, vol.4, no.4, pp.199-219, 2008

Brillouin Spectral Response Depending on Strain Non-Uniformity within Centimeter Spatial Resolution and its Application to Internal Damage Detection in Large-Scale Composite Structures

Shu Minakuchi[1], Tadahito Mizutani[1], Haruka Tsukamoto[2], Mayuko Nishio[2], Yoji Okabe[3] and Nobuo Takeda[1]

Abstract: The authors propose a technique to detect centimeter internal damages in large-scale composite structures, using an optical fiber network running throughout the structure. A Brillouin-based distributed strain sensing system with centimeter-order spatial resolution (pre-pump pulse Brillouin optical time domain analysis (PPP-BOTDA)) was utilized to detect residual non-uniform strain in the damaged area. First, Brillouin spectral response depending on the strain profile within the spatial resolution was revealed. The spectral response depending on strain non-uniformity was experimentally quantified with consideration of the general characteristics of the Brillouin gain spectrum. Then, the damage detection procedure was proposed, based on the spectral response. Finally, impact damage detection of a composite sandwich structure was numerically conducted to illustrate the effectiveness of the proposed technique. The developed system is quite useful in a first inspection of large-scale composite structures in aerospace applications.

1 Introduction

Distributed strain measurement using an optical fiber is significantly effective for monitoring the health of large-scale structures, since the strain distribution changes corresponding to the condition of the structures. Brillouin scattering-based sensing systems can measure axial strain at an arbitrary point along the optical fiber by analyzing the power spectrum of Brillouin backscattered light, which is called a Brillouin gain spectrum (BGS) [Horiguchi et al 1989, Brown et al 1999]. Several studies have utilized Brillouin-based sensing systems for the distributed strain measurement, and some techniques for detecting excessive deformation have been proposed based on shape variations of the Brillouin spectrum [DeMerchant et al 1999, Ohno et al 2002, Murayama et al 2004, Ravet et al 2006].

In general, Brillouin-based techniques estimate the value of the axial strain from the peak frequency of the BGS, and the strain is averaged over the length of spatial resolution of each system. The system with a higher spatial resolution can measure the strain distribution more precisely. Hence, the Brillouin-based technique has been continuously enhanced in regard to spatial resolution. Centimeter or millimeter spatial resolution has been realized by several innovative sensing techniques [Bao et al 1999, Kishida et al 2005, Song et al 2006]. This value is more than one order higher than that of the conventional Brillouin-based systems, and the new techniques are suitable for the global strain measurement of large-scale aerospace composite structures, where the strain intricately changes in sub-meter areas. Pre-pump pulse Brillouin optical time domain analysis (PPP-BOTDA) [Kishida et al 2005] is one such innovative technique. The commercially available system realizes 10cm spatial resolution by using an incident laser beam with a unique wave profile (Fig. 1). We have uti-

[1] Department of Advanced Energy, Graduate School of Frontier Sciences, The University of Tokyo, 5-1-5 Kashiwanoha, Kashiwa-shi, Chiba, 277-8561, Japan

[2] Department of Aeronautics and Astronautics, School of Engineering, The University of Tokyo, 7-3-1 Hongo, Bunkyo-ku, Tokyo, 113-8656, Japan

[3] Department of Mechanical and Biofunctional Systems, Institute of Industrial Science, The University of Tokyo, 4-6-1 Komaba, Meguro-ku, Tokyo 153-8505, Japan

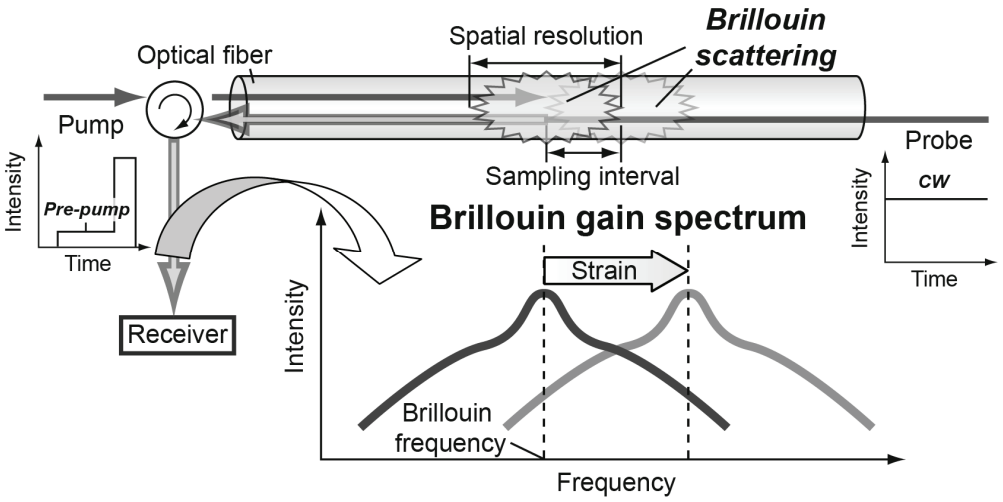

Figure 1: PPP-BOTDA sensing system.

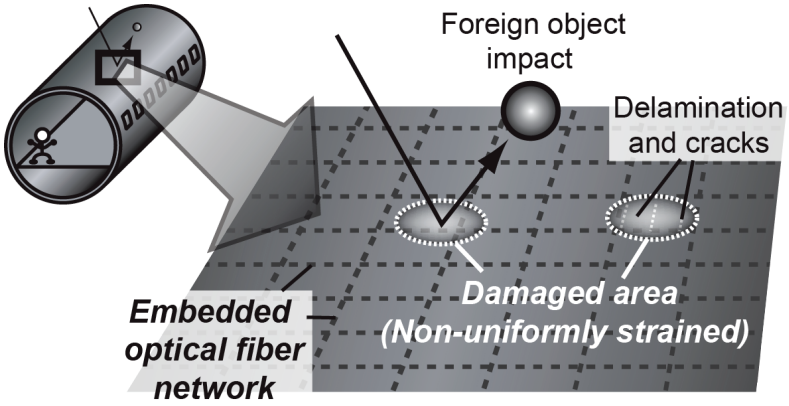

Figure 2: Schematic diagram of the damage detection technique for large-scale composite structures.

lized PPP-BOTDA with an embedded optical fiber network for measuring mechanical and thermal strain in composite structures, confirming the effectiveness of the distributed strain measurement [Mizutani et al 2006, Nishio et al 2008]. In composite materials, however, centimeter internal damages (i.e., impact damage and delamination) are critical [Abrate 1998]. Invisible internal cracks and damages significantly degrade the strength of the structures, restricting the design space of airplanes with composite materials. The Brillouin-based distributed strain measurement system has the potential to detect internal damage and improve the design and safety of the composite structure. In general, however, centimeter damages do not induce significant reduction in the stiffness of the structure, and the strain distribution around the damaged area hardly changes. Moreover, even when the damage is introduced right above the embedded optical fiber, the averaged axial strain obtained from the damaged area may not fluctuate, since the centimeter damage is negligible compared to the spatial resolution. Hence, the simple distributed strain measurement is inadequate to detect invisible damage in large-scale composite structures.

In this study, we focus on residual non-uniform strain in the damaged area. Centimeter internal damages induce permanent strain by releasing thermal residual strain [Takeda et al 2005, Minakuchi et al 2007b] or by introducing residual deformation. We measure tiny non-uniform strain by using the spectral response of the

Brillouin-based system with centimeter spatial resolution. Previous studies on the conventional Brillouin-based system demonstrated that the spectrum shape deforms due to the non-uniform axial strain and temperature within the spatial resolution, and the spectral response depending on the strain profiles was theoretically quantified [Horiguchi et al 1992, Bao et al 1993, Naruse et al 2002, Naruse et al 2003]. We utilize the analogous spectral response of PPP-BOTDA to detect centimeter damage in large-scale structures. Figure 2 depicts a schematic of the damage detection technique. The embedded optical fiber runs throughout the structure like a nerve. The optical fiber density of the network is determined from the unacceptable damage size depending on the structural site. Since the Brillouin-based system has a quite long sensing range, a limited number of optical fibers are sufficient to monitor the whole structure. When invisible damages are introduced, the non-uniform axial strain is induced within the spatial resolution, changing the Brillouin spectrum shape. Hence, we can quantitatively estimate damage size and location from the distribution of the Brillouin spectral response. The improved spatial resolution enables us to detect the centimeter damage inducing only tiny non-uniform strain.

In this paper, we begin by briefly explaining PPP-BOTDA. Next, the spectral response of PPP-BOTDA depending on the strain profile within the spatial resolution is revealed. Then, we experimentally quantify the spectral response depending on strain non-uniformity, with consideration for characteristics of the BGS. The damage detection procedure is then proposed for the first inspection of the large-scale aerospace composite structures. Finally, as an example, the spectral response to the impact damage in the composite sandwich structure is simulated, illustrating the effectiveness of the proposed technique.

2 Spectral Response of the PPP-BOTDA Sensing System

2.1 PPP-BOTDA

A schematic of the PPP-BOTDA sensing system (Neubrescope, Neubrex Co. Ltd) is illustrated in Fig. 1. This system employs a stimulated Brillouin scattering (SBS) technique. Two laser beams, a pump pulse having a unique wave profile and a continuous wave (CW) probe light, are injected into an optical fiber from both ends. Due to their different frequencies, the interaction of these two laser beams (the pre-pump and the probe light) excites acoustic waves. Then, the pulse part of the pump light is backscattered by the phonons, and part of its energy is transferred to the CW. The power gain of the CW, which is the BGS, as a function of frequency difference between the two laser beams is measured at the output end of the probe light, while the frequency of the probe light is scanned. The value of the axial strain can be estimated by measuring the peak frequency of the BGS (called Brillouin frequency), while its position along the optical fiber is calculated from the light round-trip time. This measuring system realizes a spatial resolution of 10cm, a sampling interval of 5cm, and a sensing range of more than 1km with $\pm 0.0025\%$ strain measurement accuracy.

The BGS is calculated by solving Maxwell equations with a perturbation theory [Kishida and Li 2006, Kishida et al 2004]. Figure 3 presents the model of the SBS. The probe light with the amplitude of A_{CW} is the CW from the right-hand side, and the pump light with the pre-pump can be described as follows:

$$A_p(t) = \begin{cases} A_p + C_p, & D_{\mathrm{pre}} - D \le t \le D_{\mathrm{pre}} \\ C_p, & 0 \le t \le D_{\mathrm{pre}} - D \\ 0, & \text{elsewhere} \end{cases}, \quad (1)$$

where D is the pump pulse duration and D_{pre} ($> D$) is the pre-pump duration. The amplitude of the CW probe light received at $z = 0$ is expressed as

$$E_{\mathrm{CW}}(t) = A_{\mathrm{CW}} \left| 1 + \beta H(t, \Omega) \right|. \quad (2)$$

The last term on the right-hand side of Eq. (2) represents the power gain due to the SBS, while

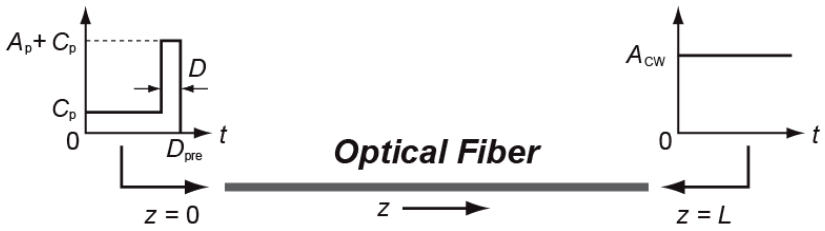

Figure 3: Model of stimulated Brillouin scattering.

β is the perturbation parameter (in this work, β = 2.2×10^{-4}), Ω is the frequency of the phonon (i.e., the difference between the frequencies of the pump and probe light), and t is time, which is related to the measuring position. In general, the SBS term $H(t,\Omega)$ is expressed by a double integral of the pump profile and a convolution of the pump profile with a phonon term. When the pump is described by the step function, as given in Eq. (1), $H(t,\Omega)$ can be split into the following four terms:

$$H(t,\Omega) = H_1(t,\Omega) + H_2(t,\Omega) + H_3(t,\Omega) + H_4(t,\Omega) \tag{3}$$

where

$$H_1(t,\Omega) = A_p^2 \int_{\frac{v_g(t-D_{\text{pre}})}{2}}^{\frac{v_g(t-D_{\text{pre}}+D)}{2}} \int_0^{t-D_{\text{pre}}+D-\frac{2z}{v_g}} h(z,s)\,ds\,dz \tag{4-1}$$

$$H_2(t,\Omega) = A_p C_p \int_{\frac{v_g(t-D_{\text{pre}})}{2}}^{\frac{v_g(t-D_{\text{pre}}+D)}{2}} \int_0^{t-\frac{2z}{v_g}} h(z,s)\,ds\,dz \tag{4-2}$$

$$H_3(t,\Omega) = A_p C_p \int_{\frac{v_g(t-D_{\text{pre}})}{2}}^{\frac{v_g(t-D_{\text{pre}}+D)}{2}} \int_0^{t-D_{\text{pre}}+D-\frac{2z}{v_g}} h(z,s)\,ds\,dz \tag{4-3}$$

$$H_4(t,\Omega) = C_p^2 \int_{\frac{v_g(t-D_{\text{pre}})}{2}}^{\frac{v_g t}{2}} \int_0^{t-\frac{2z}{v_g}} h(z,s)\,ds\,dz. \tag{4-4}$$

Here, v_g is the light wave speed in the optical fiber, and $h(z, s)$ expresses the phonon behavior:

$$h(z,s) = \Gamma \exp(-[\Gamma + i(\Omega_B(z) - \Omega)]\,s), \tag{5}$$

where Γ is the parameter related to the relaxation time of the phonon (in this study, $\Gamma/2\pi$ = 17.5MHz), and $\Omega_B(z)$ is the Brillouin frequency at position z. The Brillouin frequency $\Omega_{\text{B}}(z)$ shifts, depending on the strain and temperature applied to the optical fiber as:

$$\Omega_B(z) = 2\pi(\nu_{\text{B0}} + C_s\varepsilon(z) + C_T\Delta T(z)), \tag{6}$$

where ν_{B0} is the initial Brillouin frequency, $\varepsilon(z)$ is the axial strain along the optical fiber, $\Delta T(z)$ is the temperature change, and C_s and C_T are the proportionality constants. Finally, the power of the BGS can be expressed as:

$$V(t,\Omega) = \frac{1}{2}\beta A_{\text{CW}}^2 H(t,\Omega) + c.c. \tag{7}$$

The BGS consists of four terms, as indicated in Eqs. (3), (4), and (7). Each term physically means one of the four interactions between the phonon and the pump light. In Eq. (4), the time integral corresponds to the excitation of the phonon, and the spatial integral corresponds to the energy transfer from the pump light to the probe light (CW). Hence, the range of the spatial integral equals the spatial resolution of each term. For the PPP-BOTDA sensing system having the spatial resolution of $v_gD/2$, the term H_2 is the most important. This term represents the power gain obtained from the pulse pump light with the duration D backscattered by the phonon, which is highly excited by the pre-pump light with the duration D_{pre}. Meanwhile, the term H_4 contains the spatial information of $v_gD_{pre}/2(> v_gD/2)$, and it significantly disturbs the BGS. The term H_4 expresses

the power gain obtained from the pre-pump light backscattered by the phonon. In the PPP-BOTDA sensing system, the disturbing term is suppressed by appropriately setting the parameters of the lights; thus, high spatial resolution and measurement accuracy are realized. The general hardware settings of the PPP-BOTDA sensing system are D = 1ns, D_{pre} = 13ns, and $(A_p + C_p)/C_p$ = 25dB.

2.2 Evaluation of Spectral Response Depending on Strain Profile within Spatial Resolution

2.2.1 Materials and methods

To investigate the response of PPP-BOTDA to the non-uniform strain within the 10cm spatial resolution, we conducted a tensile test and a three-point bending test using a single specimen (Fig. 4). A polyimide-coated single-mode optical fiber (Heatop 300, Totoku Electric Co. Ltd.; ν_{Bw} = 9.56GHz, C_s = 39.4kHz/$\mu\varepsilon$) was embedded in the interface between the 6th and 7th ply of a carbon fiber reinforced plastic (CFRP) laminate (T700S/2500, Toray Industry, Inc., $[0_8]$). The specimen was loaded using a material testing system (AG-50kNI, Shimazu Co.), and the optical fiber was connected to the PPP-BOTDA sensing system (NBX-6000, Neubrex Co. Ltd.). The hardware parameters of the PPP-BOTDA system were set as "Output Pump Power" = 30dBm, "Output Probe Power" = +1dBm, "Frequency Step" = 5MHz, and "Averaging Count" = 2^{16}. This experiment was intended to clarify the effect of the strain gradient on the shape of the BGS by comparing the spectra obtained in the tensile test, where the strain distribution is uniform, and the three-point bending test, where the strain distribution is non-uniform. In both tests, the spectra were measured from the center of the specimen when the axial strain of the optical fiber at point $\varepsilon_{\max}$ was 0, 1000, 2000, and 3000$\mu\varepsilon$. In order to support the experiment theoretically, we developed a BGS simulator in LabVIEW and calculated the spectra by using Eq. (7) with consideration for the strain profiles (Eq. (6)).

2.2.2 Results

Figure 5 (a) presents the experimentally obtained spectra. For clarity, the spectra in the bending test are depicted after purposely decreasing their intensity. In the tensile test, the spectrum almost retained its shape while the peak frequency shifted to the higher frequency side, corresponding to the strain increase. In the bending test, however, the shape of the spectrum became gentle as the strain increased and the strain gradient became steep. The calculated spectra are depicted in Fig. 5 (b). The spectrum intensity was adjusted to the experimental results for a clear comparison. Even though the calculated spectrum shape did not fit with the measured one, the simulation effectively reproduced the experimental results. The steeper the strain gradient became, the more the spectrum width broadened; in contrast, the spectrum kept its shape in the tensile test.

The protruding part at the top of the measured spectrum above –1.5dB from the maximum corresponds to the term H_2 containing the information of the 10cm spatial resolution. Hence, the effect of the strain profile within the spatial resolution on the shape of the BGS can be interpreted as follows. When a uniform strain is applied, the Brillouin frequency is also uniform; thus, the BGS has only one sharp narrow peak (Fig. 6 (a)). When a non-uniform strain is introduced, however, the Brillouin frequency also becomes non-uniform, since the Brillouin frequency at each position on the optical fiber is determined by the strain at the position (Eq. (6)). As a result, the BGS consisting of the entire Brillouin scattering within the spatial resolution becomes broad (Fig. 6 (b)). Moreover, the width of the top part changes, corresponding to the non-uniformity of the strain distribution. This behavior of the BGS is analogous to that numerically presented in Ref. [Naruse et al 2002] for the conventional Brillouin-based system.

Two other characteristics were observed in the obtained spectra. First, the peak frequency shift in the bending test was smaller than the one in the tensile test, because the peak frequency is roughly determined by the averaged axial strain within the spatial resolution. Even though the values of the maximum strain $\varepsilon_{\max}$ were the same in

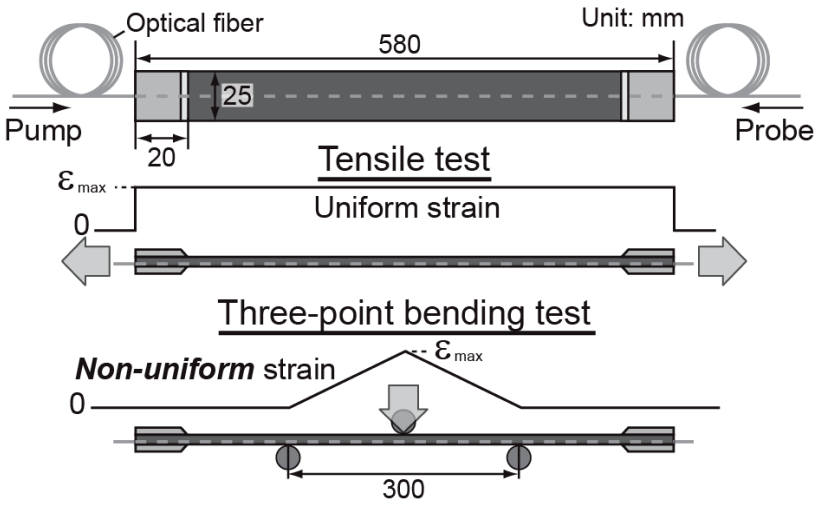

Figure 4: Specimen for evaluating the effect of strain non-uniformity on BGS.

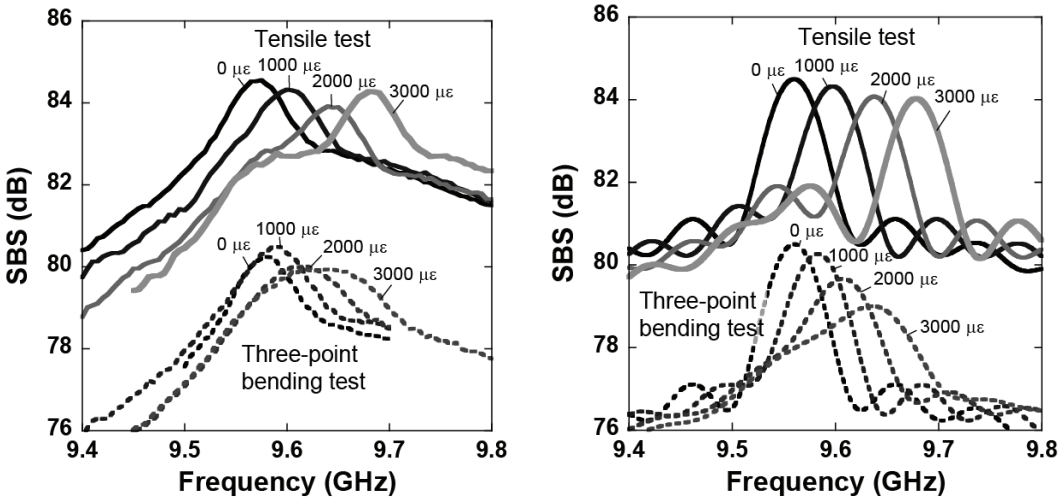

(a)Experiment. (b) Simulation.

Figure 5: Brillouin gain spectra obtained in both tests.

both tests, the strain non-uniformity in the bending test decreased the averaged strain. Hence, the peak frequency shifts in the two tests did not agree. Second, the spectra obtained in the tensile tests of $\varepsilon_{\max}$ = 2000 and 3000$\mu\varepsilon$ had a small peak at 9.6GHz (Fig. 5). This component is the term H_4 in Eq. (3). It represents the power gain obtained from the backscattered pre-pump light, which is ahead of the pump pulse light, and has spatial information of $v_g D_{pre}/2$ = 130cm. Since the length of the specimen was 58cm, the BGS measured from the center of the specimen contained the backscattered pre-pump light from 100cm unloaded optical fiber ahead of the measured area, making a small confusing peak at the initial Brillouin frequency (ν_{Bw} = 9.56GHz). This is one of the most important characteristics of the BGS obtained by PPP-BOTDA.

As clarified above, the BGS deforms depending on the strain profile within the centimeter spatial resolution. When the large-scale composite structures is damaged (Fig. 2), a non-uniform strain is induced along the optical fiber embedded in the damaged area, changing the BGS correspond-

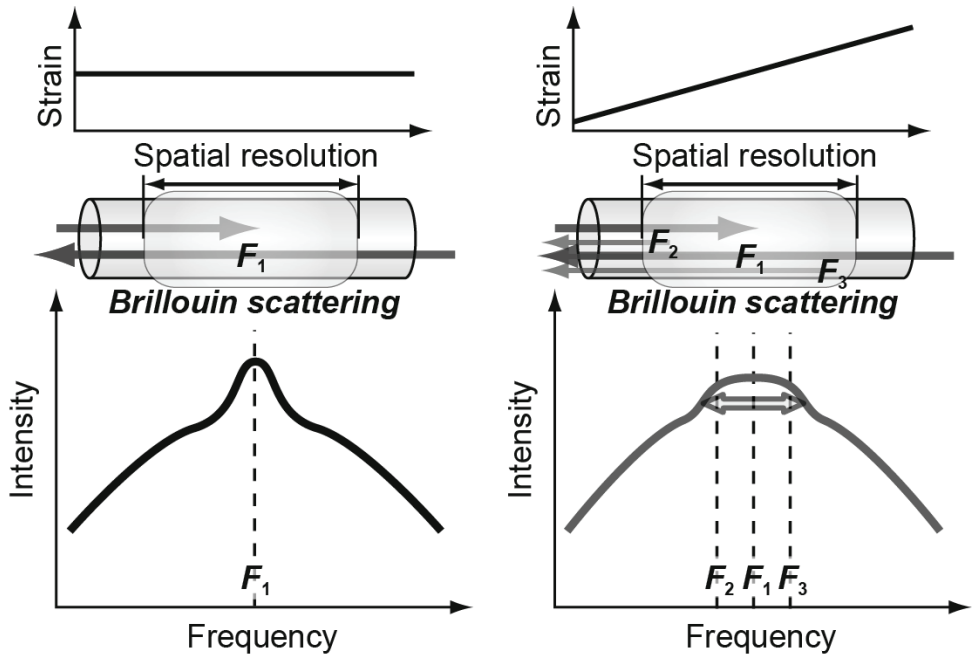

(a) Uniform strain. (b) Non-uniform strain.

Figure 6: Schematic of Brillouin scattering depending on strain profile within spatial resolution.

ing to the severity of the damage. Before applying the spectral response to the damage detection scheme, however, we must evaluate the spectral response depending on strain non-uniformity, both qualitatively and quantitatively. Experimental investigation is essential to determine the detection limit and to estimate the damage size and severity from the measured spectral response. In the next section, we discuss a beam-bending test with a bonded optical fiber that was conducted to evaluate the spectral response depending on the linear strain gradient, which represents one of the fundamental non-uniform strain changes. Specifically, the focus is on the width of the BGS. Some characteristics of the spectrum width are revealed and discussed.

3 Qualitative and Quantitative Evaluation of Spectral Response Depending on Strain Non-Uniformity

3.1 Materials and Methods

The width of the BGS depending on the strain gradient was evaluated. In this study, we selected a full width at –0.5dB from maximum $F_{-0.5dB}$ as a representative value of the spectrum width (Fig. 7). We chose this width because the protruding part at the top of the measured spectrum above -1.5dB from the maximum corresponds to the term H_2 containing the information of the 10cm spatial resolution, as mentioned above. An automatic program written in Matlab calculated $F_{-0.5dB}$ from the measured power spectra by using least-squares approximation polynomials (Fig. 7).

The experimental setup was developed based on the following findings obtained in a preliminary test using an unloaded optical fiber (Heatop 300, Totoku Electric Co. Ltd.).

1. The mean value of the spectrum widths along the whole optical fiber varies in each measurement with the same hardware settings, possibly due to the instability of the pump and probe lasers. The intensity and the frequency stabilities of the two incident lights differ in each measurement.

2. The relative value of the spectrum width in

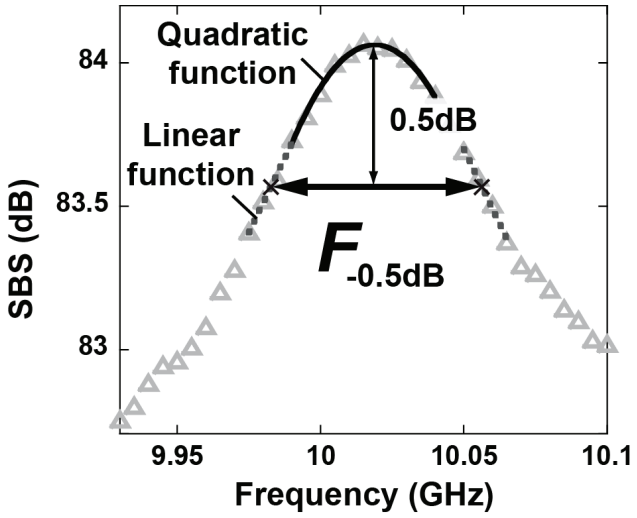

Figure 7: Definition of $F_{-0.5dB}$ representing spectrum width.

each measurement depends on the position on the optical fiber, possibly due to the intrinsic nonhomogeneity of the optical fiber. The minimal fluctuation in the physical and optical parameters along the optical fiber may disturb uniform Brillouin scattering.

We organized the experiment with consideration for the two general characteristics of the spectrum width. Figure 8 depicts a schematic of the experimental set-up. The bonded optical fiber was divided into part *A* and part *B*. The optical fiber in part *A* was non-uniformly loaded under the three-point beam bending condition and used for the quantification of $F_{-0.5dB}$ depending on the magnitude of the strain gradient. However, the optical fiber in part *B* was utilized to evaluate the instability of the pump and probe lasers in each measurement. Three key points were involved in the experimental setup.

1. The optical fiber in part *A* was adhered on the sanded bottom surface of the acrylic beam specimen using a two-component epoxy adhesive. In order to obtain multiple data in each measurement, 20 bonded parts were introduced. The optical fiber was arrayed in the bonded part to apply the same strain distribution. Based on the spatial resolution of 10cm and the measurement point uncertainty, we set the length of the bonded parts to 20cm and obtained one spectrum from the center of one bonded part. The bonded parts were separated with loose fibers of 150cm to eliminate the influence on the obtained spectra from the neighboring bonded part. We quantitatively evaluated $F_{-0.5dB}$ depending on the strain gradient and investigated the positional dependence due to the optical fiber nonhomogeneity.

2. To achieve accurate quantification of the spectral response depending on the strain non-uniformity within the 10cm spatial resolution, the optical fiber in part *A* was bonded in a uniform tension state. As indicated in section 2.2.2, the BGS of the PPP-BOTDA system contains a small confusing component induced by the backscattered pre-pump light, which is related to the term H_4. Since the component contains 130cm spatial information, it significantly disturbs the "true" spectral response depending on strain non-uniformity within the 10cm spatial resolution. In the bending test with the bonded optical fiber (Fig. 8), the confusing part is backscattered from the unloaded loose fiber. In order to eliminate the disturbance, the Brillouin frequency ranges of the bonded

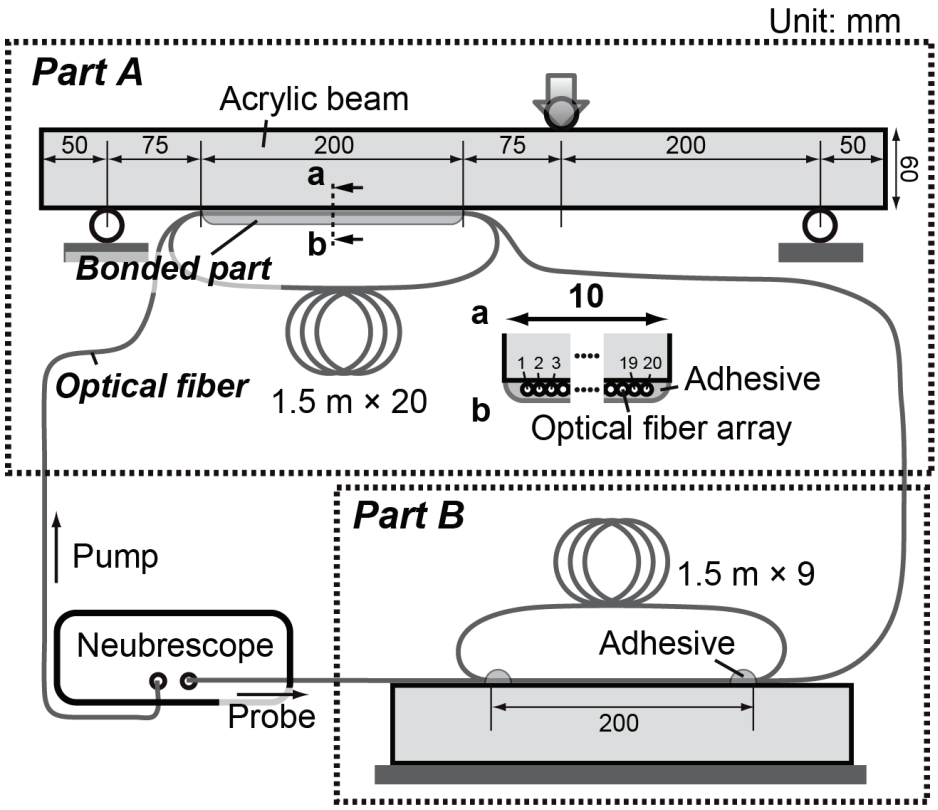

Figure 8: Experimental setup for evaluating spectrum width depending on strain non-uniformity.

fiber and the loose fiber must be substantially separated. Thus, we applied uniform 1% pre-tension strain in the bonded fiber. Figure 9 depicts the BGS obtained from one of the bonded parts. The "true" component obtained from the 10cm spatial resolution was successfully insulated from the confusing part.

3. The optical fiber in part *B* was similarly bonded on the surface of another acrylic beam, and the constant strain of 1% was applied. Nine bonded parts were introduced. As indicated above, spectrum width changes due to the instability of the incident lights. We obtained the mean value of $F_{\text{-0.5dB}}$ from the nine parts in each measurement. The value might somewhat represent the instability of the two lasers at the frequency range of the applied strain of 1%. We investigated the correlation between the non-uniformly loaded part *A* and the uniformly loaded part *B*, and clarified the effect of the instability of the lasers on the spectral response.

Electrical-resistance strain gauges were also bonded on the two beam specimens to measure the strain distribution along the bonded optical fiber. We obtained the spectra when the strain gradient in the bonded part in part *A*, D_ε, was 0, 500, 1000, 2000, and 3000$\mu\varepsilon$/10cm. The hardware parameters of the PPP-BOTDA system (NBX-6020, Neubrex Co. Ltd.) were set as “Output Pump Power” = 25dBm, "Output Probe Power" = +1dBm, and “Averaging Count” = 2^{14}. Except for the strain gradient D_ε of 3000$\mu\varepsilon$/10cm, we repeated the measurement of each strain gradient 10 times. Meanwhile, five times measurements were conducted for the condition of D_ε = 3000$\mu\varepsilon$/10cm. The experiment was conducted at a constant room temperature.

3.2 Results and Discussion

All the spectrum widths $F_{\text{-0.5dB}}$ obtained from the 45 measurements are plotted in Fig. 10. Ex-

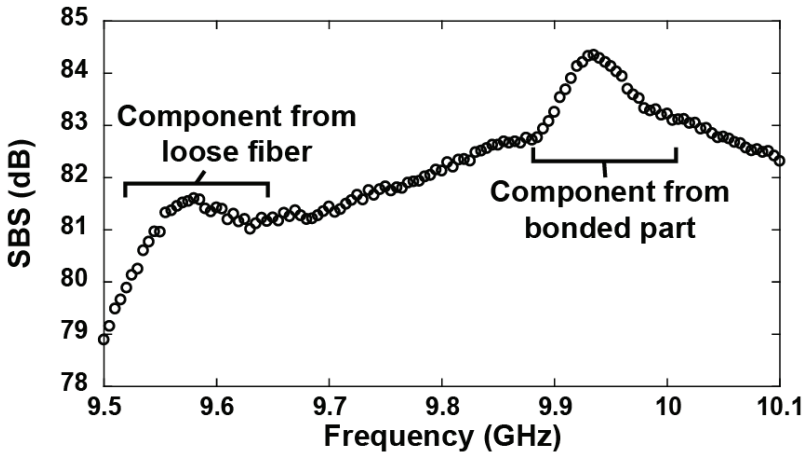

Figure 9: Brillouin gain spectrum obtained from bonded part.

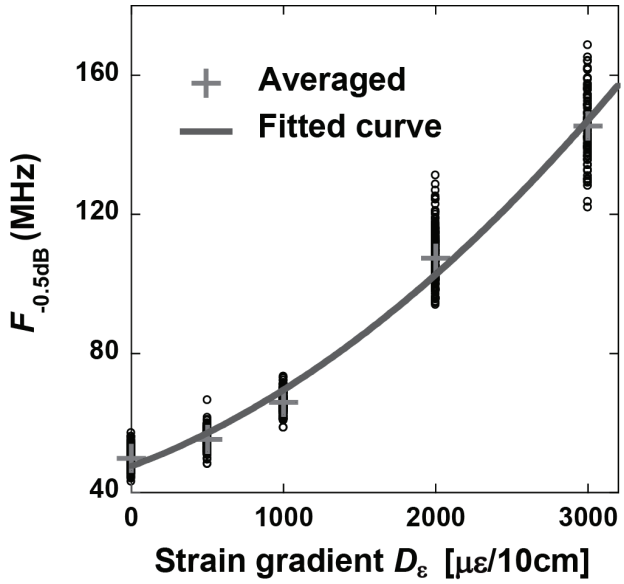

Figure 10: Measured spectrum width depending on strain gradient.

cept for the strain gradient D_ε of $3000\mu\varepsilon$/10cm, each strain gradient had 200 data points, which were obtained from the 20 bonded parts in the 10 times measurements. Figure 10 indicates that we can roughly determine the strain gradient from the measured spectrum width. The averaged spectrum width $\overline{F_{-0.5\mathrm{dB}}}$ increased nonlinearly with the strain gradient. A quadratic function fitted well with the increasing tendency (Fig. 10):

$$\overline{F_{-0.5\mathrm{dB}}} = a_0 \times D_\varepsilon^2 + a_1 \times 10^{-2} \times D_\varepsilon + a_2 \quad (8)$$

$$[a_0 = 5.6 \times 10^{-6},\ a_1 = 1.5 \times 10^{-2},\ a_2 = 47.5\ ]^{\cdot}$$

The coefficients a_0, a_1, and a_2 were derived by the least-squares method. The strain non-uniformity also multiplied the data spread, and some outliers were generated. The standard deviations of the spectrum widths are listed in Table 1. It is important to note that the data points at D_ε = $1000\mu\varepsilon$/10cm had $F_{\text{-0.5dB}}$ values clearly different from the ones at the uniformly loaded state (D_ε = $0\mu\varepsilon$/10cm). Therefore, when the strain

Table 1: Standard deviations of spectrum widths at each strain gradient.

Strain gradient ($\mu\varepsilon$/10cm)	0	500	1000	2000	3000
Standard deviation (MHz)	2.65	2.62	2.78	7.25	9.56

gradient is larger than $1000\mu\varepsilon$/10cm, we can almost certainly detect the non-uniformly strained position with only one measurement. Conversely, $1000\mu\varepsilon$/10cm may be the limiting value of the linear strain gradient to detect strain non-uniformity by the single measurement with the PPP-BOTDA system used in this study. Hence, the minimum detectable damage is defined by the damage inducing the $1000\mu\varepsilon$/10cm strain non-uniformity. However, multiple measurements can more precisely and sensitively quantify the non-uniform strain. As indicated in Fig. 10, the mean value of the spectrum width $\overline{F_{-0.5\mathrm{dB}}}$ obtained by the multiple measurements increased at the strain gradient of less than $1000\mu\varepsilon$/10cm, enabling us to detect strain non-uniformity even at the strain gradient of a few hundred $\mu\varepsilon$/10cm. Although multiple measurements require considerable time, they must significantly improve the sensitivity of the damage detection.

Meanwhile, as indicated above, the measured spectra are affected by a number of factors. Each value of $F_{-0.5\mathrm{dB}}$ obtained in the experiment can be divided into four parts:

$$F_{-0.5\mathrm{dB}} = F^{\mathrm{true}}_{-0.5\mathrm{dB}} + E_{\mathrm{position}} + E_{\mathrm{time}} + E_{\mathrm{system}} + E_{\mathrm{others}}, \quad (9)$$

where $F^{\mathrm{true}}_{-0.5\mathrm{dB}}$ is the true value of $F_{-0.5\mathrm{dB}}$ depending on only the magnitude of the strain gradient, E_{position} is the error associated with the optical fiber nonhomogeneity, E_{time} is the error caused by the instability of the pump and probe lasers at each measurement time, E_{system} is the error due to the other system instabilities, and E_{others} is the error induced by changes in experimental conditions and other factors. Here, $F^{\mathrm{true}}_{-0.5\mathrm{dB}}$ might agree exactly with the average of the measured values $\overline{F_{-0.5\mathrm{dB}}}$ (Fig. 10). The four error terms disperse the data and complicate the quantitative estimation of the strain non-uniformity.

First, we investigated the effect of E_{position} on the spectral response. Figure 11 compares $F_{-0.5\mathrm{dB}}$ obtained from each of the 20 bonded parts. Bonded parts Nos. 1 and 20 correspond to both edges of the optical fiber array (Fig. 8), and the data points in the same measurement have the same style. When D_ε was $0\mu\varepsilon$/10cm, even though the uniform 1% pre-tension strain was applied to the optical fiber, the averaged spectrum widths $\overline{F_{-0.5\mathrm{dB}}}$ at the 20 bonded parts varied widely compared to the data spreads at each bonded part. The spectrum widths had clear positional dependency. We believe this result arose from optical fiber nonhomogeneity, which is related to E_{position}. The minimal fluctuation in the physical and optical parameters must have disturbed the uniform Brillouin scattering, and surprisingly, when the strain gradient was $500\mu\varepsilon$/10cm, $\overline{F_{-0.5\mathrm{dB}}}$ at each bonded part still had similar positional dependency. This result indicates that optical fiber nonhomogeneity significantly affects the spectral response to the non-uniform strain. However, the spectral response gradually lost optical fiber-based positional dependency as the strain gradient increased to more than $1000\mu\varepsilon$/10cm. The bonded parts near both edges of the optical fiber array tended to have large values of $F_{-0.5\mathrm{dB}}$, possibly due to the imperfection of the specimen with the bonded optical fiber. The loading state of the fiber array differed, depending on the position in the cross-width direction; thus, the same non-uniform strain was not induced at all 20 bonded parts. This confusing positional dependency grew stronger as the applied load increased, and the differences between the magnitudes of the strain gradient at each bonded part increased. Thus, in high strain gradient states, the error due to the specimen-based positional dependency, which is classified into E_{others}, became dominant, making it difficult to evaluate the effect of optical fiber-based positional dependency on the spectral response. However, consideration of optical fiber nonhomogeneity must improve the quality of the obtained data at the small strain gradient. In order to correct the error E_{position}, we introduced the following unique

parameter P_i^{position} to the bonded part No. i (i = 1, 2, . . . , 20):

$$P_i^{\text{position}} = \frac{\frac{1}{10}\sum_{j=1}^{10} F_{-0.5\text{dB}\,ij}}{\frac{1}{200}\sum_{i=1}^{20}\sum_{j=1}^{10} F_{-0.5\text{dB}\,ij}} \quad (\text{at} \quad D_\varepsilon = 0\,[\mu\varepsilon/10\text{cm}]), \quad (10)$$

where $F_{-0.5\text{dB}\,ij}$ is the spectrum width obtained from bonded part No. i in the measurement j (j = 1, 2, . . . , 10) at $D_\varepsilon = 0\mu\varepsilon$/10cm. The numerator on the right-hand side is the averaged spectrum widths $\overline{F_{-0.5\text{dB}}}$ at bonded part No. i in the 10 measurements, and the denominator is the mean value of all the obtained $F_{-0.5\text{dB}}$. This non-dimensional value represents the optical fiber nonhomogeneity at each bonded part. We eliminated the effect of E_{position} on the spectral response by compensating the obtained $F_{-0.5\text{dB}}$ at the bonded part No. i with the following simple equation:

$$\langle F_{-0.5\text{dB}} \rangle = \frac{F_{-0.5\text{dB}}}{P_i^{\text{position}}}. \quad (11)$$

Figure 12 compares $F_{-0.5\text{dB}}$ and $\langle F_{-0.5\text{dB}} \rangle$. At the strain gradient D_ε of 0 and 500$\mu\varepsilon$/10cm, the compensated spectrum width had a narrower range of values and the outlier disappeared, confirming the importance of considering optical fiber nonhomogeneity. The standard deviation of the compensated spectrum width at D_ε of 0$\mu\varepsilon$/10cm was 2.13MHz, and that at D_ε of 500$\mu\varepsilon$/10cm was 2.73MHz. At D_ε of 1000$\mu\varepsilon$/10cm, however, the value range broadened with the compensation. The specimen-based positional dependency, which was independent of the optical fiber-based positional dependency, became dominant at the strain gradient of more than 1000$\mu\varepsilon$/10cm. Thus, the compensation based on E_{position} somewhat degraded the data quality. Further tests with an improved experimental setup are needed for the accurate quantification of the spectral response in the high strain gradient state. It is also important to note that the data spread at each bonded part increased with the strain gradient (Fig. 11). This result probably had two causes. First, the non-uniform strain might have destabilized the Brillouin scattering, disturbing the stability of the Brillouin spectrum width. Second, the strain gradient reduced the peak intensity of the BGS; thus, the spectrum became noisy, making it difficult to calculate the spectrum width based on the method depicted in Fig. 7.

Next, we investigated the effect of E_{time} on the spectral response. As explained above, E_{time} is induced by the instability of the two lasers in each measurement. We began by introducing the following two values in each measurement:

$$\overline{F^A_{-0.5\text{dB}}} = \frac{1}{20}\sum_{i=1}^{20} \langle F_{-0.5\text{dB}\,i} \rangle,$$
$$\overline{F^B_{-0.5\text{dB}}} = \frac{1}{9}\sum_{k=1}^{9} F^B_{-0.5\text{dB}\,k} \quad (12)$$

The former is the average of the compensated spectrum widths $\langle F_{-0.5\text{dB}\,i} \rangle$ obtained from all the bonded parts No. i (i = 1, 2, . . . , 20) in part A, where the non-uniform strain was introduced. The effects of the optical fiber- and specimen-based positional dependency are eliminated by the averaging. The latter is the mean value of the spectrum widths $F^B_{-0.5\text{dB}\,k}$ ($F_{-0.5\text{dB}}$) obtained from all bonded parts No. k (k = 1, 2, . . . , 9) in part B, where the 1% uniform tensile strain was applied. The effect of the optical fiber-based positional dependency is eliminated by the averaging. It somehow represents the instability of the two lasers in each measurement. We evaluated the correlation between $\overline{F^A_{-0.5\text{dB}}}$ and $\overline{F^B_{-0.5\text{dB}}}$ to clarify the effect of the instability on the spectral response depending on the strain gradient. Figure 13 depicts the relationship between the two values of each measurement. The correlation factors (CFs) are also presented. When the strain gradient D_ε was less than 1000$\mu\varepsilon$/10cm, $\overline{F^A_{-0.5\text{dB}}}$ had a high correlation with $\overline{F^B_{-0.5\text{dB}}}$, confirming that the instability of the probe and pump lasers significantly affects the spectral response. At the strain gradients of 2000 and 3000$\mu\varepsilon$/10cm, however, the two values were poorly correlated. This result may be due to the difference between the strain magnitudes in parts A and B, adding to the two aforementioned causes for the data spread at the high strain gradients. Even though the 1% tensile strain

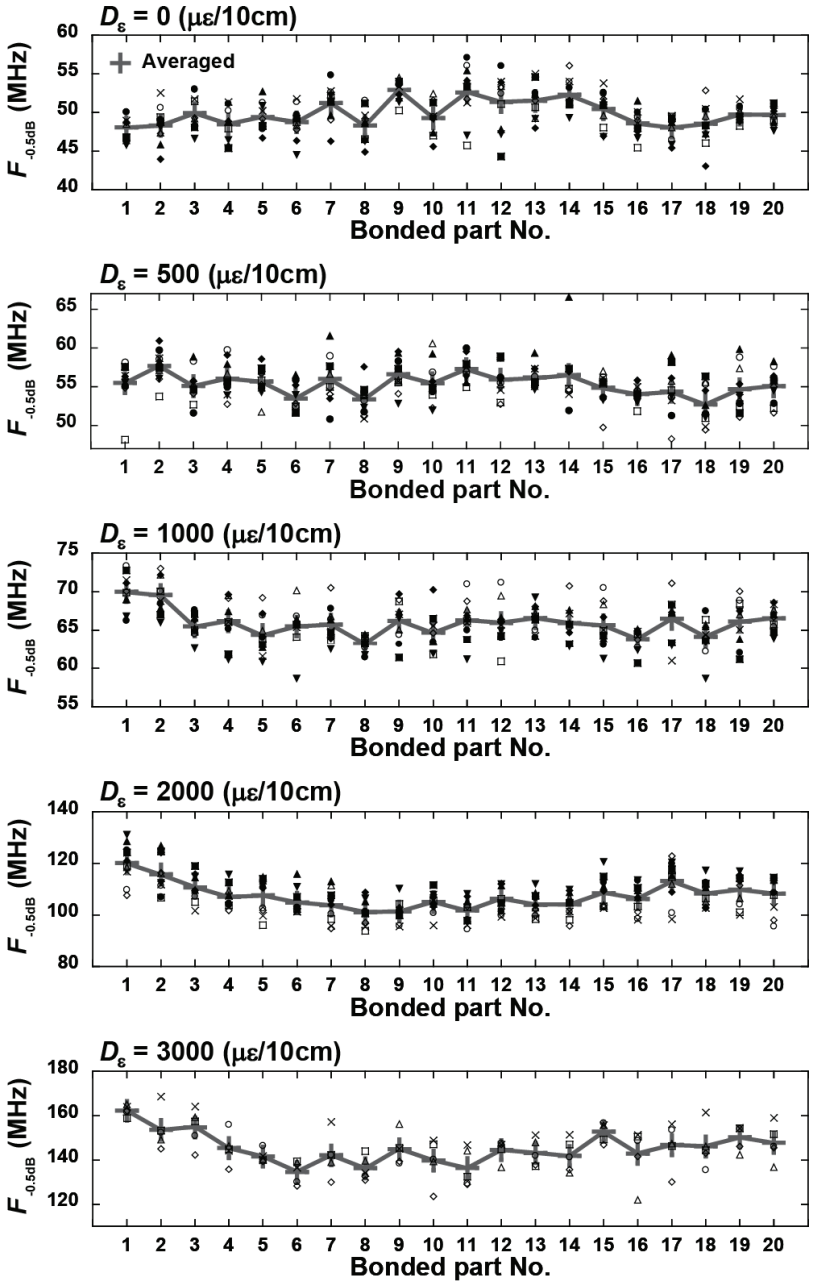

Figure 11: Spectrum width at each bonded part depending on strain gradient.

in part B was kept constant throughout the experiment, the strain in part A increased with an increase in the strain gradient, and finally became more than 1.5% when $D_\varepsilon = 3000\mu\varepsilon$/10cm. Since $\overline{F^B_{-0.5\mathrm{dB}}}$ represented the instability of the lasers at the frequency range corresponding to the 1% tensile strain, the value was not appropriate to be compared to $\overline{F^A_{-0.5\mathrm{dB}}}$ at the high strain gradient. In order to evaluate the correlation between the instability of the lasers and the spectral response depending on strain non-uniformity, we should have measured the spectra at a similar frequency range. Finally, we corrected the error E_{time} at the strain gradient of less than $1000\mu\varepsilon$/10cm by introducing the following normalization in the measurement l

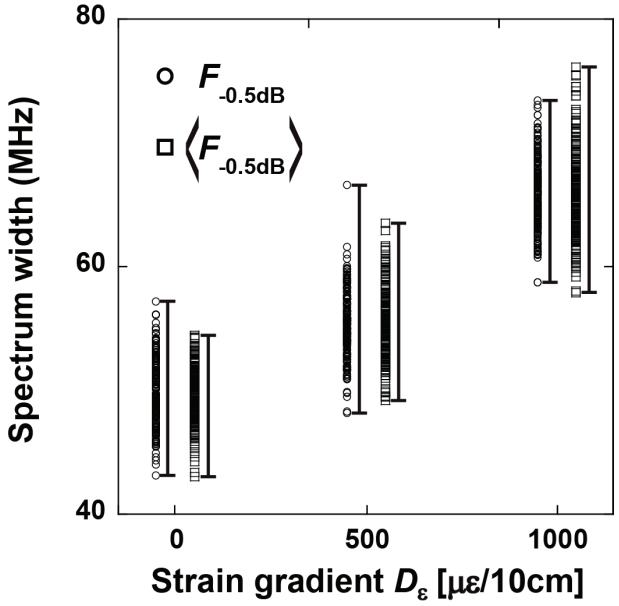

Figure 12: Comparison between uncompensated and compensated spectrum widths.

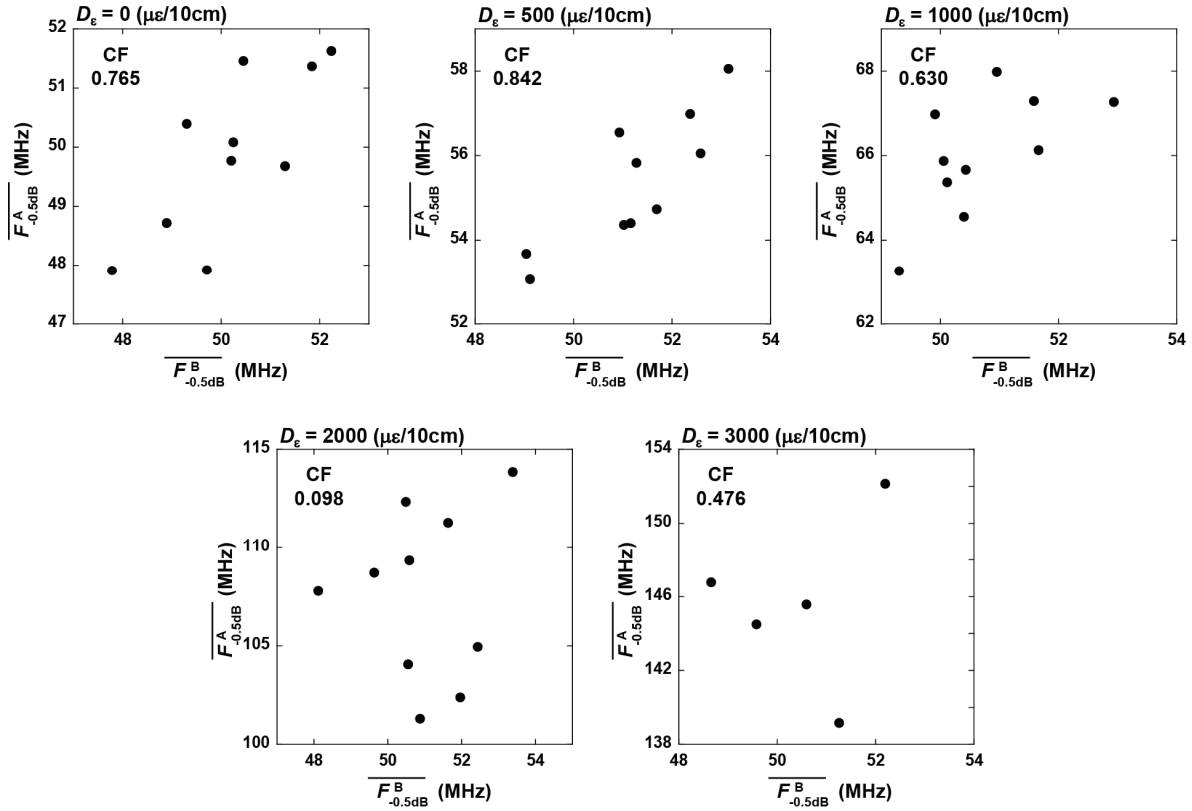

Figure 13: Relationship between instability of lasers and spectral response depending on strain non-uniformity.

(l = 1, 2, ..., 45):

$$\langle \mathrm{NW} \rangle = \frac{\langle F_{-0.5\mathrm{dB}} \rangle}{\overline{F^B_{-0.5\mathrm{dB}\,l}}}. \qquad (13)$$

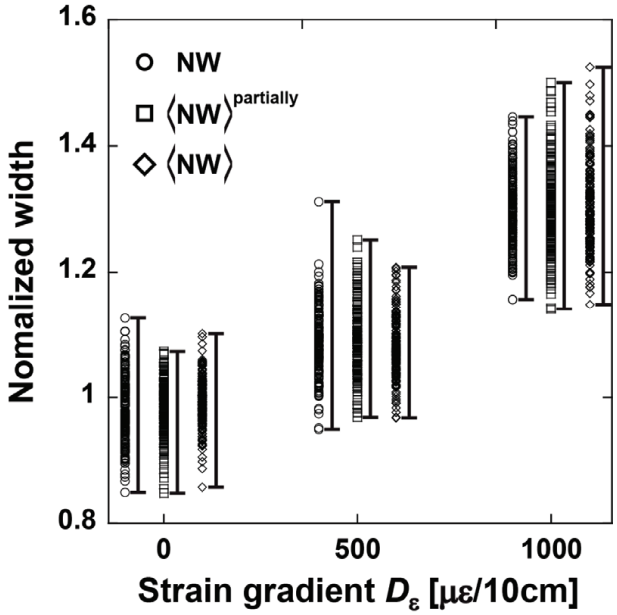

Figure 14: Comparison between variously normalized spectrum widths.

The denominator of the right-hand side represents the instability of the lasers in the measurement l. Figure 14 compares the normalized value with the following benchmarks:

$$\langle \mathrm{NW} \rangle^{\mathrm{partially}} = \frac{\langle F_{-0.5\mathrm{dB}} \rangle}{\frac{1}{45} \sum_{l=1}^{45} \overline{F^B_{-0.5\mathrm{dB}\, l}}}, \qquad \mathrm{NW} = \frac{F_{-0.5\mathrm{dB}}}{\frac{1}{45} \sum_{l=1}^{45} \overline{F^B_{-0.5\mathrm{dB}\, l}}}. \tag{14}$$

The denominators on the right-hand sides express the true value of the spectrum widths at the frequency range corresponding to the 1% tensile strain. The effect of the instability is eliminated by the averaging. In Fig. 14, data quality was further improved at $D_\varepsilon = 0$ and $500\mu\varepsilon$/10cm, compared to Fig. 12. The standard deviations of each normalized spectrum width are listed in Table 2. Again, however, the effect of the specimen-based positional dependency was strong at the strain gradient of 1000ε/10cm, and the compensation broadened the value range of the data. Further experimental investigation is required to clarify the effect of the instability of the lasers at the high strain gradient.

To conclude this section, we both quantitatively and qualitatively evaluated the spectral response depending on the strain gradient within the centimeter spatial resolution. It was revealed that the spectrum width $F_{\text{-}0.5\mathrm{dB}}$ quadratically increased with the strain gradient, and we could roughly determine the strain non-uniformity from the measured spectra. Moreover, the data analysis confirmed the importance of considering the optical fiber nonhomogeneity and the instability of the pump and probe lasers. The compensation of the related errors significantly improved the data quality of the spectral response. Many issues must be addressed in the future study of damage detection. First, a rigorous statistical approach to estimate precisely the magnitude of the strain non-uniformity should be established. Since the reliability of damage detection depends on the accuracy of the non-uniformity estimation, a highly reliable damage detection system is essential to quantify the non-uniform strain from the measured spectrum responses, which varies widely (Fig. 13), using their statistical properties. Second, the spectral response depending on other strain profiles must be clarified. Even though the linear strain is one of the fundamental strain profiles, the residual strain distribution within the damaged composite material is not always simple.

Table 2: Standard deviations of normalized spectrum widths.

	0 [$\mu\varepsilon$/10cm]	500 [$\mu\varepsilon$/10cm]
NW	0.052	0.052
$\langle \mathrm{NW} \rangle^{\mathrm{partially}}$	0.042	0.054
$\langle \mathrm{NW} \rangle$	0.038	0.047

Investigation of the equivalence between the linear strain profile and the other complicated ones is a key issue that must be addressed; moreover, new indicators of the Brillouin spectrum shape representing the strain non-uniformity within the spatial resolution should be proposed. Finally, the factors causing the error E_{system} must be determined. In this study, we intensively investigated the effects of the optical fiber nonhomogeneity and the instability of the lasers. However, as indicated in Fig. 14, many other factors destabilize the spectral response. A more sophisticated compensation must be conducted based on the newly identified error factors, enabling a more accurate estimation of strain non-uniformity.

In the next section, we discuss the damage detection technique based on the spectral response. A specific procedure for detecting internal damage in the large-scale composite structures is presented. In order to illustrate the effectiveness of the proposed technique, we simulated the spectral response to impact damage in the composite sandwich structure.

4 Damage Detection Technique Using Spectral Response to Non-Uniform Strain

4.1 Damage Detection Procedure

A specific procedure is presented in Fig. 15. First, the spectra are measured throughout the embedded optical fiber (Fig. 2). The measurement is conducted before or after the operation of the structure. Second, the representative value of each spectrum width is automatically calculated for the quantitative evaluation of the strain non-uniformity at each measurement point. For multiple measurements, the averaged value of the spectrum widths is utilized. When the damage is introduced, only the damaged area has unusually large values of the spectrum width, depending on the extent of the damage. This is because severe damage induces wider and higher non-uniform residual strain inside the structures. Hence, on the basis of the spectral response investigated in the previous sections, we can rapidly estimate the damage location and size from the distribution of the spectrum widths along a single optical fiber. This intuitive system is quite useful in the first inspection of the large-scale composite structures. Based on the obtained information, we can determine an appropriate action for safe and efficient operation (e.g., a later repair, a more accurate inspection, or an emergency repair).

The compensation of the aforementioned two errors due to the characteristics of the BGS will improve the sensitivity and accuracy of the damage detection technique. The error E_{position} may be corrected by evaluating the nonhomogeneity of the optical fiber before the embedment. Furthermore, the error E_{time} is supposed to be eliminated by using a calibration fiber, which is connected to the embedded sensing fiber for estimating the instability of the incident lasers. It is also important to note that the structure with no damage is deformed by its own weight and the applied loads, introducing the non-uniform strain in the structures to some degree. Specifically, the connection parts are highly loaded, and the strain changes sharply around them. Hence, even when the structure is not damaged, the true value of the spectrum width varies at each measurement point. In order to detect the tiny non-uniform strain induced by the internal damage, it is crucial to measure the distribution of the spectrum widths from the undamaged structure and establish a baseline value at each measurement point. The difference between the measured value and the baseline indicates the existence and extent of the damage.

In the final section, we conduct a response simulation of the proposed technique to impact damage

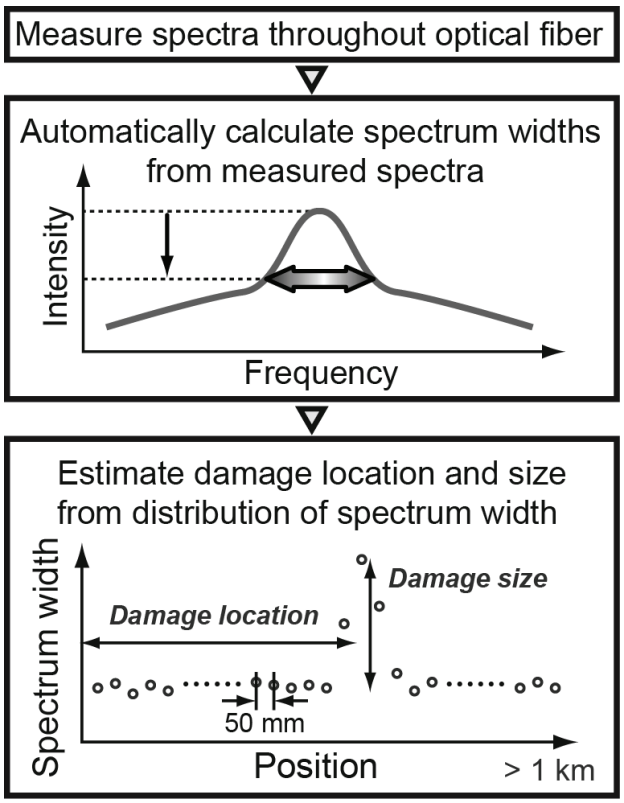

Figure 15: Damage detection procedure for large-scale composite structures.

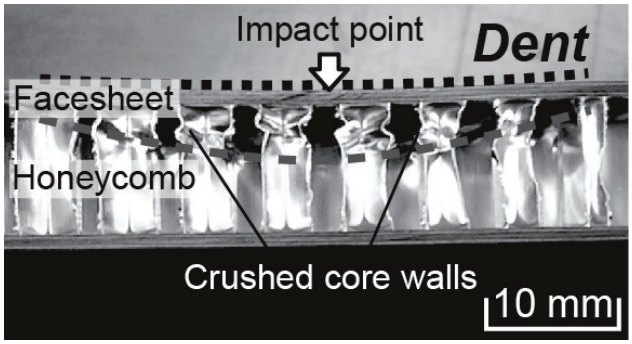

Figure 16: Cross-sectional view of impact damage in composite sandwich structures.

in the composite sandwich structure. The non-uniform strain induced by a residual facesheet dent is detected with the use of the spectral response.

4.2 Detection of Impact Damage in Composite Sandwich Structures

The composite sandwich structure is an integral construction consisting of two composite facesheets and a thick lightweight core [Zenkert 1997]. Composite sandwich structures are widely utilized in aerospace structures because of their excellent mechanical properties. However, since the facesheet is thin and the lightweight core is weak, they can easily be damaged when a localized transverse impact or indentation load is applied [Abrate 1998]. The crushed core under the loading point induces a barely visible residual facesheet dent (Fig. 16), significantly degrading the mechanical proper-

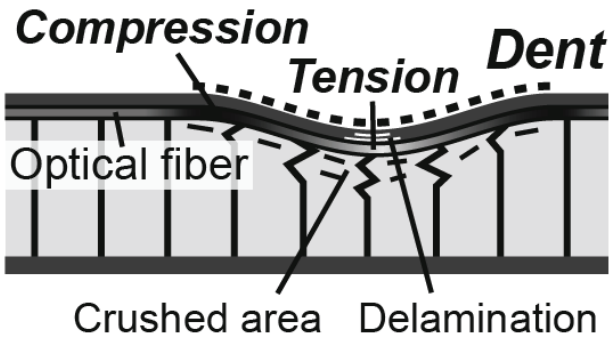

Figure 17: Schematic of impact damage detection technique.

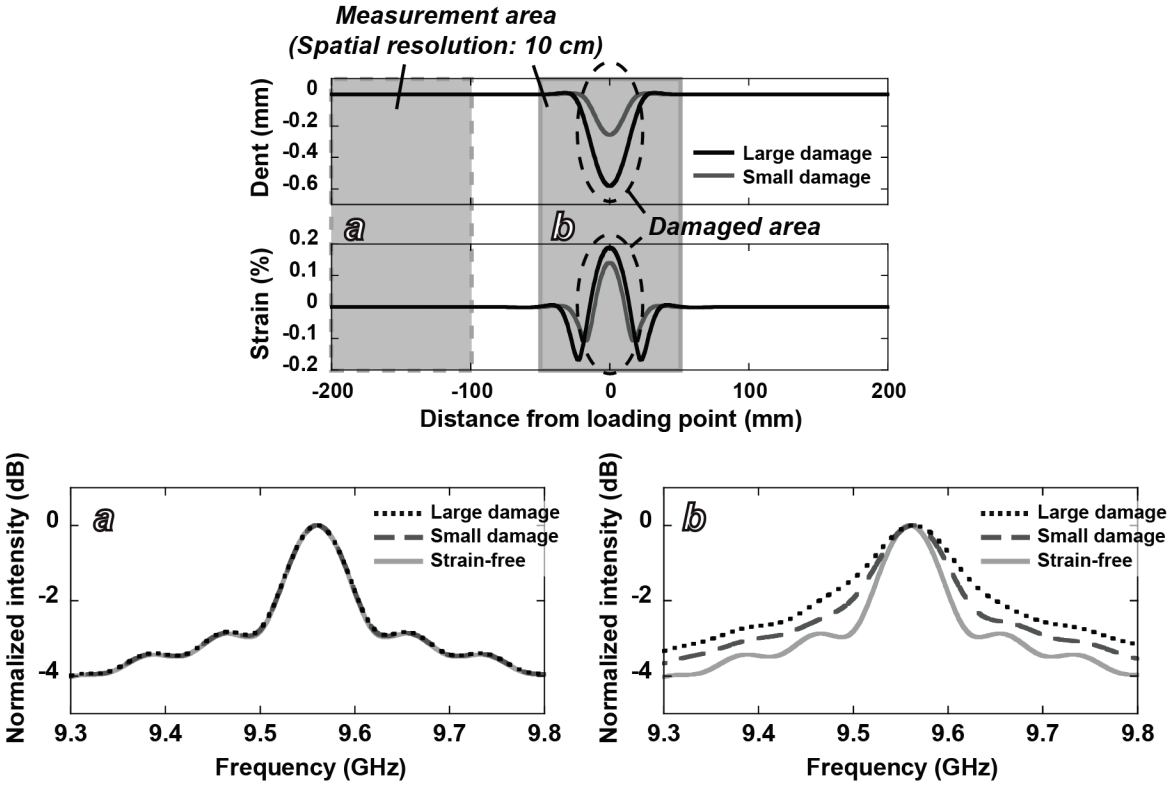

Figure 18: Brillouin gain spectra obtained from different measurement areas.

ties of the structure. Meanwhile, the dent introduces a non-uniform strain along its concavo-convex shape [Minakuchi et al 2007b]. The residual strain of more than $1000\mu\varepsilon$ remains on the facesheet even with barely visible damage. We utilize the Brillouin spectral response to detect the non-uniformly strained area for impact damage detection. Figure 17 presents a schematic of this technique. The optical fiber is embedded in the adhesive layer between the facesheet and the core [Minakuchi et al 2007a], and measures the strain along the bottom surface of the composite facesheet. Hence, the facesheet dent induces tensile and compressive axial strain along the embedded optical fiber at its concave and convex parts. This non-uniform strain changes the spectral response; thus, the impact damage can be detected.

We introduced two kinds of residual facesheet dents, which had unequal size smaller than the spatial resolution of 10cm, in a sandwich beam

consisting of the CFRP facesheets (T700S/2500, Toray Industry, Inc.; $[0_8]$), an aluminum honeycomb core (AL 3/16-5052-.001, Showa Aircraft Industry Co.; thickness: 20mm), and thermoplastic adhesive films (AF-163-2K, 3M Co.) [Minakuchi et al 2007b]. The change of the BGS due to large and small damage was predicted by using the strain calculated with a "segment-wise model," which was developed for theoretical simulation of the facesheet dent formation in the composite sandwich beams [Minakuchi et al 2008]. The segment-wise model can accurately calculate the non-uniform strain distribution along the surface of the dented facesheet. Figure 18 presents the spectra obtained from different measurement areas. The intensity of each spectrum is normalized by the intensity of the highest component. The spectrum in a strain-free state is also used as a reference. The graphs above the spectra plot the calculated facesheet dent displacement and the axial strain distribution along the embedded optical fiber. When the measurement area was not damaged (area *a*), the shape of the BGS did not change, since the strain distribution was uniform. In the damaged area (area *b*), however, the spectra became broader because of the non-uniform strain along the facesheet dent. And the width of the spectrum broadened corresponding to the damage size, since larger damage generated higher and wider non-uniform strain along the residual facesheet dent. It is also important to note that the peak frequency of the BGS, which is proportional to the measured strain, did not change, even though the damage was introduced at the center of the measurement area. This was because the damage size was less than the spatial resolution of 10cm and the average of the non-uniform axial strain along the facesheet dent was almost zero. That is to say, simple strain monitoring is inadequate to detect centimeter damage. Only the spectral response can indicate damage occurrence.

It was confirmed that the proposed damage detection system is quite sensitive to both damage location and size. In the near future, this technique will be validated through a verification experiment. Further study to apply the proposed damage detection procedure to delamination monitoring for composite laminates is also planned.

5 Conclusions

The authors developed a technique to detect centimeter internal damages in large-scale composite structures, using Brillouin spectral response to non-uniform strain within the centimeter spatial resolution. First, the spectral response was both quantitatively and qualitatively evaluated by the experiment organized with consideration of the characteristics of the BGS. The spectrum width quadratically increased with strain non-uniformity, and the data analysis confirmed the importance of considering the optical fiber nonhomogeneity and the instability of the lasers of the sensing system. The damage detection procedure was then proposed. The distribution of the spectral response along the sensing optical fiber was utilized to estimate the damage size and location. Finally, as an example, impact damage detection of the composite sandwich structure was numerically conducted to illustrate the effectiveness of the proposed technique.

Acknowledgement: The authors are grateful to Che-Hsien Li (Neubrex Co. Ltd.) for many fruitful discussions on the subject.

References

Abrate S. (1998): *Impact on composite structures*. Cambridge University Press.

Bao X, Brown A, DeMerchant M, Smith J. (1999): Characterization of the Brillouin-loss spectrum of single-mode fibers by use of very short (< 10-ns) pulses. *Optics Letters* 24(8):510-512.

Bao X, Webb DJ, Jackson DA. (1993): Temperature Non-uniformity in Distributed Temperature Sensors. *Electronics Letters* 29(11):976-978.

Brown AW, DeMerchant MD, Bao XY, Bremner TW. (1999): Spatial resolution enhancement of a Brillouin-distributed sensor using a novel signal processing method. *Journal of Lightwave Technology* 17(7):1179-1183.

DeMerchant M, Brown A, Bao XY, Bremner T. (1999): Structural monitoring by use of a Brillouin distributed sensor. *Applied Optics* 38(13):2755-2759.

Horiguchi T, Kurashima T, Tateda M. (1989): Tensile strain dependence of Brillouin frequency shift in silica optical fibers. *Photonics Technology Letters, IEEE.* 1(5):107-108.

Horiguchi T, Kurashima T, Tateda M, Ishihara K, Wakui Y. (1992): Brillouin Characterization of Fiber Strain in Bent Slot-Type Optical-Fiber Cables, *Journal of Lightwave Technology* 10(9):1196-1201.

Kishida K, Li CH. (2006): Pulse pre-pump-BOTDA technology for new generation of distributed strain measuring system. *Structural Health Monitoring and Intelligent Infrastructure* (Ou, Li & Daun, editor). Taylor & Francis, 471-477.

Kishida K, Li CH, Lin S, Nishiguchi K. (2004): Pulsed pre-pump method to achieve cm-order spatial resolution in Brillouin distributed measuring technique. *Technical Report of IEICE* OFT104(341):15-20.

Kishida K, Li CH, Nishiguchi K. (2005): Pulse pre-pump method for cm-order spatial resolution of BOTDA. *Proceeding of the SPIE* 5855:559-562.

Mizutani T, Nishi T, Takeda N. (2006): Distributed sensing technique for large-scale composite structures with embedded small-diameter optical fibers, *Proceeding of 18th International Conference on Optical Fiber Sensors*, ThE15.

Minakuchi S, Okabe Y, Takeda N. (2007a): Real-time detection of debonding between honeycomb core and facesheet using a small-diameter FBG sensor embedded in adhesive layer. *Journal of Sandwich Structures and Materials*, 9(1):9-33.

Minakuchi S, Okabe Y, Takeda N. (2007b): "Segment-wise model" for theoretical simulation of barely visible indentation damage in composite sandwich beams: Part II - Experimental verification and discussion. *Composites Part A: Applied Science and Manufacturing*, 38(12):2443-2450.

Minakuchi S, Okabe Y, Takeda N. (2008): "Segment-wise model" for theoretical simulation of barely visible indentation damage in composite sandwich beams: Part I - Formulation. *Composites Part A: Applied Science and Manufacturing,* 39(1):133-144.

Murayama H, Kageyama K, Naruse H, Shimada A. (2004): Distributed strain sensing from damaged composite materials based on shape variation of the Brillouin spectrum. *Journal of Intelligent Material Systems and Structures* 15(1):17-25.

Naruse H, Tateda M, Ohno H, Shimada A. (2002): Dependence of the Brillouin gain spectrum on linear strain distribution for optical time-domain reflectometer-type strain sensors. *Applied Optic*, 41(34): 7212-7217.

Naruse H, Tateda M, Ohno H, Shimada A. (2003): Deformation of the Brillouin gain spectrum caused by parabolic strain distribution and resulting measurement error in BOTDR strain measurement system. *IEICE Transactions on Electronics* E86C(10):2111-2121.

Neubrex Co., Ltd. http://www.neubrex.jp

Nishio M, Horii S, Takeda N. (2008): Deformation monitoring of unsymmetric laminates using Brillouin type distributed strain sensing system with embedded optical fiber network, *Proceeding of the US-Japan conference on composite materials*, P-4.

Ohno H, Naruse H, Kurashima T, Nobiki A, Uchiyama Y, Kusakabe Y. (2002): Application of Brillouin scattering-based distributed optical fiber strain sensor to actual concrete piles. *IEICE Transactions on Electronics* E85C(4):945-951.

Ravet F, Zou LF, Bao XY, Chen L, Huang RF, Khoo HA. (2006): Detection of buckling in steel pipeline and column by the distributed Brillouin sensor. *Optical Fiber Technology* 12(4):305-311.

Song KY, He ZY, Hotate K. (2006): Distributed strain measurement with millimeter-order spatial resolution based on Brillouin optical correlation domain analysis. *Optics Letters* 31(17): 2526-2528.

Takeda S, Minakuchi S, Okabe Y, Takeda N. (2005): Delamination monitoring of laminated composites subjected to low-velocity impact using small-diameter FBG sensors. *Composites Part A: Applied Science and Manufacturing*, 36(7):903-908.

Zenkert D, editor. (1997): *The handbook of sandwich construction*. EMAS Publishing.